Georgia Journal of Science

Volume 77 *No. 2 Scholarly Contributions from the Membership and Others* | Article 11

2019

The South Polar Region of Mars: A Review

Richard W. Schmude Jr.
Gordon State College, schmude@gordonstate.edu

The South Polar Region of Mars: A Review

Acknowledgements
ACKNOWLEDGEMENTS The writer would like to thank the individual at the 2018-GRAM meeting who suggested a large dust storm deposited dust, which is a possible cause of the Cryptic Terrain.

THE SOUTH POLAR REGION OF MARS: A REVIEW

Richard W. Schmude, Jr., Gordon State College, Barnesville, Georgia, 30204

ABSTRACT

This review summarizes mostly Earth-based observations of Mars' south polar region (SPR) made since the late 17th century along with measurements of the 2003, 2005, and 2018 south polar cap (SPC). There are four conclusions. The first one is the SPC has not underwent radius changes exceeding 3 % and 10 % for L_s < 230° and L_s = 230°–270°, respectively, in at least the last 125 years. Secondly, *t* test results are consistent with the SPC being larger when on the morning terminator than on the afternoon terminator. Thirdly, the dark area Depressio Magna drawn by Antoniadi (1975) and the "cryptic terrain" described by Kieffer et al. (2000) are probably the same feature. Fourthly, isolated clouds, away from the disk edges and terminators, are scarce in the SPR during L_s = 180°–330°.

Keywords: Mars, south polar region, south polar cap, cryptic terrain

INTRODUCTION

Certain abbreviations are used here and are summarized in Table I. In this paper, our knowledge of Mars' SPR from a global perspective is summarized. Global perspective is a term used to mean the view as seen from Earth. The south polar region encompasses the ice cap and nearby cloud systems. Areas south of ~45° S are included in the SPR. The areocentric longitude of the Sun, as seen from Mars (L_s), describes the seasonal date. For the southern hemisphere the beginning of fall, winter, spring, and summer correspond to L_s = 0°, 90°, 180°, and 270°, respectively.

Table I. A summary of common abbreviations used in this review

Abbreviation	Meaning
SPR	South Polar Region
NPR	North Polar Region
SPC	South Polar Cap
SPH	South Polar Hood
MY	Mars Year; each Mars year starts at L_s = 0°
Novus Mons	Mountains of Mitchel
MGS	Mars Global Surveyor
MRO	Mars Reconnaissance Orbiter

This review presents up-to-date results of Mars' SPR. It attempts to answer four questions: Has the SPC changed in size and appearance over the last 125 years? Is there a difference in SPC measurements when it is on the afternoon and morning terminators? What are the characteristics of the dark area within the SPC in the early spring? and What is the frequency of white clouds in the SPR?

In many cases, using the MY instead of the year on the Gregorian calendar makes trends easier to follow. Each new MY begins at L_s = 0°; MY one started on April 11, 1955. The start date for each new MY on the Gregorian calendar is given in Piqueux et al. (2015).

Values of L_s are often stated to give the reader a sense of the Martian season. These are obtained from the Astronomical Almanac and from the Jet Propulsion Laboratory (JPL) New Horizons website at https://ssd.jpl.nasa.gov/horizons.cgi.

Major historical discoveries related to the SPR are summarized in Table II. One discovery of importance is the drawing of Mars' SPC by Huygens on August 13, 1672 (L_s = 250°) or Mars year –150. This drawing shows a blunt end on the eastern side of the SPC, which is consistent with modern trends of the shrinkage of the SPC (James et al. 2001). In 1845, Mitchel describes a dark spot within the SPC in 1845 or Mars year –58; this is a second, noteworthy discovery (Barnard 1895). This feature has been observed on several occasions since then and is undoubtedly the "cryptic terrain" (Kieffer et al. 2000). Antoniadi (1975) reports observing it from L_s = 207°–236° in 1924.

The terminator shows the boundary between day and night. Before opposition, when Mars is opposite from our Sun, Earth-based observers see Mars' afternoon terminator. After opposition, observers see Mars' morning terminator. This may not be the case for spacecraft images. This distinction is important because temperatures are lower on the morning than afternoon terminator. Consequently, ground frosts and surface fogs are more likely to be seen near the morning terminator. Dust clouds, however, are more likely to be seen near the afternoon terminator.

MATERIALS & METHODS

Images made at resolutions near 50 km/pixel are the basis of this review. In most cases, images were analyzed using WinJUPOS (Hahn 2019). Images from the Mars Color Imager (MARCI) weather report website (Malin et al. 2018a) were not used for SPC measurements because they were not made from Earth. Uncertainties in Earth-based images are discussed in the *results* section.

In a few cases, linear fits of data were carried out. A *t* test, at the 95 % confidence level, was used to determine if a correlation coefficient of a linear fit is statistically significant (Larson and Farber 2006). Correlation coefficients were computed from Microsoft Excel for each linear fit. The larger the data scatter, the more difficult it is to measure small changes over time. Data scatter is partly caused by uncertainties and, hence, these are now discussed.

There are several sources of uncertainty in SPC measurements. The largest may be insufficient resolution. Before 1988, measurements were made either visually or from photographs, micrometers, or reticles. These were usually limited by atmospheric turbulence (Dobbins et al. 1988). Typical uncertainties may have been around 1 arcsec. In the rare cases, where seeing was excellent, measurements were often limited by the Dawes limit (Dobbins et al. 1988). During excellent seeing conditions, uncertainties may have dropped to 0.5 arcsec. This meant random error exceeded 100 km. Since the 1990s, digital images, with modern processing techniques, have become widely available. The best Earth-based digital images today show more detail than the best photographs from the 1950s (Slipher 1962, plate XII); therefore, uncertainties of SPC measurements from digital images have decreased to perhaps 0.3 arcsec or less, leading to uncertainties of ~2° of latitude.

Table II. Major historical events related to the south polar region of Mars

Year	Event	Source
1659	SPC and SPH first noticed	Dick (1838), p. 118 who cites Maraldi
1672	Huygens draws an asymmetrical SPC	Flammarion 2015, p. 28
1704	Maraldi observes two bright polar patches	Flammarion 2015, p. 32
1719	Maraldi observes the SPC is not centered on the South Pole	McKim 1999, p. 15
1781-83	Herschel establishes orientation of Mars' rotational axis	Herschel (1784)
1798	Olbers notes the SPC has variations in brilliancy	Flammarion 2015, p. 56
1798	Schröter observes SPC almost blending in to disk edge; he also makes early measurements of the SPC size	Flammarion 2015, p. 57 and Slipher (1962)
1837	Early measurements of SPH by Beer & Madler	Flammarion 2015, p. 460
1839	Galle draws irregular SPH	Flammarion 2015, p. 108
1845	Mitchel draws dark patch in SPC; notes large ice patch separating from SPC	Barnard (1895)
1880	Early dust storm noted in Thaumasia; SPC appears yellow	McKim (1999), p. 24 & 135
1892-94	Barnard makes early micrometer measurements of SPC	Barnard (1895, 1903)
Early 1900s	Existence of cloud mantles in SPR during autumn/winter	De Vaucouleurs (1954) p. 201 & Slipher (1962), p. 22
1956	Kuiper notes the brightness ratio of SPC to desert is lower in red than blue	Kuiper (1957)
1969	Mariner 6 and 7 measure temperature and spectrum of SPC; the results are consistent with a frozen carbon dioxide SPC	Collins (1971), pp. 20–21
1988	Observers report the effect of phase on the appearance of the SPC	Beish et al. 1991
1999-2003	Shrinking SPC shows little change in size during Mars years 24, 25, and 26	Benson and James (2005)
2000	Cryptic terrain identified as not being bare ground	Kieffer et al. (2000)
~2000	Seasonal map of SPH compiled based on measurements taken near 1400 hours local time	Wang and Ingersoll (2002)

A second source of uncertainty is Mars' phase. Mars' phase angle may reach 47°. This introduces two problems. The phase defect, which is the portion of Mars' disk not receiving sunlight, may cover part or all of the SPC rendering at least part of it not entirely visible. Consequently, WinJUPOS may give erroneous results. Secondly, the SPC may become darker at the edge closest to the phase defect. Notice the SPC is darker near the phase defect in Figures 1A compared to Figure 1D when Mars is at opposition. This darkening may lead to an underestimation of SPC size. Phase darkening may be one reason for the underestimation of SPC size from my 1988 observations (Schmude 1989) and the SPC sizes reported by Antoniadi (1975). In fact, Beish et al. (1991) report that before opposition in 1988, the afternoon side of the SPC was consistently duller than the center or morning side. This was not reported after opposition. Therefore, this group already observed and reported phase darkening.

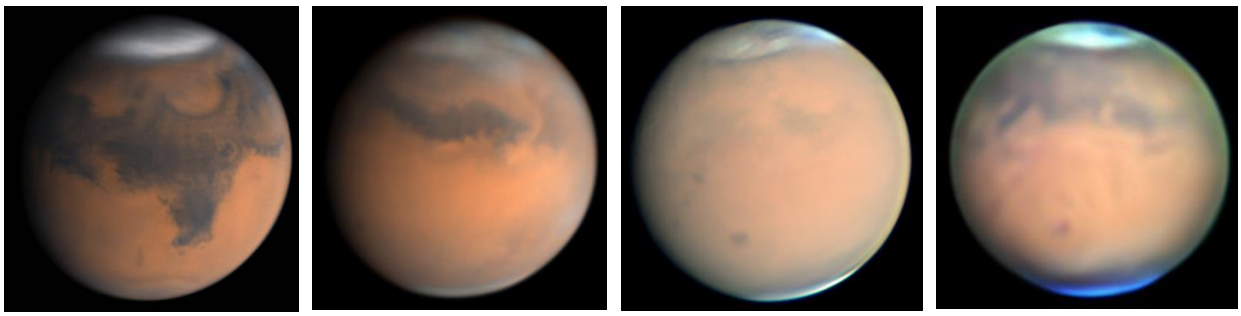

A **B** **C** **D**

Figure 1. Images of Mars showing phase darkening and a white cloud on the morning edge of the SPC. South is at the top in all images. **A**: June 8, 2018 (7:55.8 UT) by D. Peach; **B**: June 18, 2018 (7:49.7 UT) by D. Peach; **C**: July 5, 2018 (16:45.2 UT) by A. Wesley; **D**: July 27, 2018 (5:16.6 UT) by M. Hood.

A third source of uncertainty is the presence of the large dark features Depressio Magna and Rima Australis (Antoniadi 1975, fig. 135) within the SPC. One may see these in Figures 1A, 1C, and 1D. These may lead to an underestimation of cap size.

Condensate and dust clouds may also affect SPC measurements. During mid-2018, a large and bright morning cloud developed at the SPC edge. See Figure 1B and 1C. It may have developed from atmospheric dust. Clouds covering the SPC edge may lead to errors. Deposited dust may also lead to error since it leaves a dark outer coating (Schmude 2018a). This would lead to a smaller SPC size estimate. Ground frost and clouds, near the SPC edge, may also be the reason why the SPC appears larger on the morning terminator than when it is on the afternoon terminator. This is discussed later.

Another source of uncertainty is the noncircular shape of the SPC along with it not being centered on the South Pole. Lowell drew maps of the shrinking SPC in his original book first published in 1895 (Lowell 2002). Uncertainties arising from these characteristics were reduced using a three-parameter model, which is described in the next section.

RESULTS

The analysis of recent SPC results are first presented. Discussions of the early spring (L_s < 230°) and late spring (L_s > 230°) SPC are then reviewed. These cover measurements made between 1798 and 2018. Discussions of the SPH, other white clouds, and dust

activity are then given. Finally, bright dusty craters and the SPC size on the morning and afternoon terminators are discussed.

Over 400 images were analyzed in the 2018 SPC studies. A sample of images made between L_s = 210 and 214° was examined to determine mean trends in seeing; exposure time and altitude of Mars at the time images were made. The mean seeing, exposure time, and altitude were (5 on a scale of 1 to 10) and 0.008 s and 38°, respectively. In many cases, observers took at least several hundred images, stacked them, carried out a derotation routine, and presented a final image.

The writer fitted his 2003, 2005, and 2018 data to the three-parameter model described by James and Lumme (1982) and (Iwasaki et al. 1986b). Essentially, mean cap radii were measured for each 4° increment of L_s. The selected x_o, y_o, and r values gave the lowest value of $(r - r_i)^2$ where r is the mean cap radius (in planetary radii) and r_i is the radius for the specific x_i, y_i values used at a given longitude. The cap center is described by x_o and y_o. The x_i and y_i values giving the lowest value of $(r - r_i)^2$ became the selected x_o and y_o values. The recent results are summarized in Tables IIIA (2003) and IIIB (2005 and 2018). Essentially, a least squares routine was carried out to find the best fit of x_o, y_o and r for each data set. For L_s < 230°, the x_i and y_i values were adjusted in increments of 0.001 planetary radii over the range of –0.01 to +0.01. (The approximate equivalence is 0.009 planetary radii equals one degree of latitude.) For L_s > 230°, the increments were increased as described in Tables IIIA and IIIB. Mean SPC radii, in degrees of latitude, are also given. The $(r - r_i)^2$ were examined for L_s = 210°–214° and L_s = 246°–250° for 2018. The values near the one giving the best fit had $(r - r_i)^2$ value nearly the same values. It is for this reason estimated uncertainties of 0.005 and 0.010 units of planetary radii are selected for the x_o and y_o values in Table IIIA and IIIB for L_s < 230° and L_s > 230°, respectively.

The longitude and latitude of the SPC center were determined using measurements made between 1956 and 2018. The mean values of x_o and y_o were combined into increments of L_s starting with L_s = 180.1°–230.0°. The results are summarized in Table IV. Before L_s = 230°, the y_o values are small and positive whereas the x_o values are small and negative. Bear in mind the positive y-axis is 0° W and the negative x-axis is 90° W (Iwasaki et al. 1986b). After L_s = 230°, the values of x_o and y_o are farther from zero, which is consistent with the cap center being farther from the South Pole. This change is consistent with historical records (Herschel 1784; Slipher 1962, p. 16; Antoniadi 1975, p. 47; Lowell 2002, Plate II).

Values of x_o and y_o were transformed into degrees of longitude and latitude. Essentially this involved a conversion from rectangular to polar coordinates. The resulting values are summarized in Table IV. The uncertainty in SPC location in Table IV is one to two degrees in latitude. The uncertainty in longitude depends on the latitude. For example, at 84° S, an uncertainty of 60 km corresponds to 1° of latitude, but 10° of longitude. It is concluded the center of the SPC is near the south pole until L_s = 230°. Afterwards the cap center shifts farther away from the pole in the general direction of 30°±°10 W.

In the writer's opinion, astronomers have made reliable measurements of the SPC since the late eighteenth century. These are compared to the spacecraft results measured in 1999 by James et al. (2001). Theirs is considered a landmark study because it is based on Mars Global Surveyor images made from a nearly polar orbit. This discussion is broken into two seasonal periods, which are before L_s = 230° and after L_s = 230°.

Table IIIA. Results of my 2003 SPC measurements being fitted to the three-parameter circle model described by James and Lumme (1982) and Iwasaki et al. (1986b).[a] The sample standard deviation values for r and the radius are in parentheses.

L_s	x_o[b]	y_o[b]	r (planetary radii)	SPC Radius (degrees)
190°–194°	–0.002	0.006	0.289 (0.007)	32.2 (0.7)
194°–198°	0.002	–0.008	0.285 (0.007)	31.8 (0.7)
198°–202°	–0.008	0.003	0.266 (0.005)	29.8 (0.6)
202°–206°	–0.001	0.005	0.262 (0.007)	29.4 (0.7)
206°–210°	–0.002	0.005	0.247 (0.005)	27.7 (0.6)
210°–214°	0.003	–0.007	0.247 (0.006)	27.7 (0.6)
214°–218°	–0.003	0.000	0.231 (0.005)	26.0 (0.5)
218°–222°	–0.004	–0.002	0.224 (0.005)	25.3 (0.6)
222°–226°	0.001	0.003	0.211 (0.005)	23.8 (0.5)
226°–230°	0.000	0.003	0.200 (0.007)	22.6 (0.8)
230°–234°	0.005	0.000	0.187 (0.008)	21.2 (0.9)
234°–238°	–0.005	0.010	0.175 (0.011)	19.9 (1.3)
238°–242°	–0.005	0.015	0.161 (0.012)	18.3 (1.3)
242°–246°	–0.005	0.015	0.157 (0.015)	17.8 (1.7)
246°–250°	–0.005	0.030	0.149 (0.013)	16.9 (1.4)
250°–254°	–0.021	0.056	0.112 (0.025)	13 (2.8)
254°–258°	–0.035	0.040	0.099 (0.010)	11.3 (1.1)
258°–262°	–0.035	0.049	0.086 (0.007)	9.8 (0.8)
262°–266°	–0.035	0.049	0.088 (0.006)	10.1 (0.7)
266°–270°	–0.028	0.049	0.084 (0.007)	9.6 (0.8)
270°–274°	–0.035	0.040	0.083 (0.007)	9.5 (0.7)
274°–278°	–0.020	0.040	0.073 (0.009)	8.4 (1.0)
278°–282°	–0.020	0.030	0.063 (0.006)	7.2 (0.7)
282°–286°	–0.020	0.040	0.064 (0.009)	7.3 (1.0)
286°–290°	–0.005	0.025	0.054 (0.006)	6.2 (0.7)

[a]In all cases, the x_i and y_i values yielding the lowest value of $(r - r_i)^2$ are the selected x_o and y_o values, respectively.

[b]The x_i and y_i values were changed in increments of 0.007 planetary radii over the range of –0.07 to 0.07 for L_s = 250°–254° and 258°–270°. All other values after L_s = 230° were changed in increments of 0.005 planetary radii over the range of –0.05 to 0.05. The values for L_s = 190°–230° were changed in increments of 0.001 planetary radii over the range of –0.01 to 0.01.

Before L_s = 230°

Table V summarizes SPC size studies carried out since 1798 excluding the multi-apparition studies of Fischbacher et al. (1969) and Beish (2012), which are considered separately. The Table V footnotes describe the details. The two-tailed Wilcoxon signed-rank test, at the 95 % confidence level, was carried out to determine if there is a statistically significant difference between results of a certain year and those in 1999 (Larson and Farber 2006, p. 577). Some years show a statistically significant difference while others do not. These results are discussed later.

The mean differences in SPC radii, relative to 1999, are also given in Table V. These are plotted against the year, and the results are shown in Figure 2A. An estimated

uncertainty of 0.9° was selected for all values based on several factors. The coefficient of determination (r^2) is 0.0669, which means the correlation coefficient (r) is 0.2587 from the linear fit. A two-tailed *t* test at the 95 % confidence level was carried out to determine if the correlation coefficient is significant. The results are not statistically significant (Larson and Farber 2006, p. 466).

Table IIIB. Results of my 2005 and 2018 SPC measurements being fitted to the three-parameter circle model described by James and Lumme (1982) and Iwasaki et al. (1986b).[a] The sample standard deviation values for r and the radius are in parentheses.

	2005 apparition			
L_s	**x_o**[b]	**y_o**[b]	**r (planetary radii)**	**SPC Radius (degrees)**
274°–282°	–0.005	0.020	0.068 (0.004)	7.8 (0.5)
282°–290°	–0.010	0.020	0.073 (0.008)	8.4 (0.9)
290°–298°	0.000	0.015	0.065 (0.003)	7.4 (0.3)
298°–306°	–0.005	0.010	0.058 (0.007)	6.6 (0.8)
306°–314°	–0.005	0.000	0.043 (0.005)	4.9 (0.6)
314°–322°	–0.005	0.020	0.030 (0.004)	3.4 (0.5)
	2018 apparition			
L_s	**x_o**[b]	**y_o**[b]	**r (planetary radii)**	**SPC Radius (degrees)**
186°–190°	–0.008	0.001	0.288 (0.005)	32.1 (0.5)
190°–194°	–0.007	–0.004	0.272 (0.007)	30.4 (0.7)
194°–198°	–0.005	–0.003	0.262 (0.006)[d]	29.4 (0.6)
198°–202°	0.006	0.002	0.254 (0.007)	28.5 (0.8)
202°–206°	–0.001	0.006	0.253 (0.008)[e]	28.4 (0.9)
206°–210°	–0.002	0.000	0.245 (0.005)	27.5 (0.5)
210°–214°	–0.003	0.006	0.233 (0.006)	26.2 (0.7)
214°–218°	–0.004	0.010[c]	0.227 (0.005)	25.6 (0.5)
218°–222°	–0.002	0.007	0.225 (0.004)	25.4 (0.4)
222°–226°	–0.004	0.003	0.208 (0.005)	23.5 (0.5)
226°–230°	–0.004	0.005	0.198 (0.008)	22.4 (0.9)
230°–234°	–0.005	0.005	0.186 (0.006)	21.1 (0.7)
234°–238°	–0.005	0.010	0.176 (0.007)	20.0 (0.8)
238°–242°	0.000	0.005	0.166 (0.010)	18.9 (1.1)
242°–246°	–0.010	0.015	0.152 (0.009)	17.3 (1.0)
246°–250°	–0.005	0.025	0.144 (0.009)	16.4 (1.0)

[a]In all cases, the x_i and y_i values yielding the lowest value of $(r - r_i)^2$ are the selected x_o and y_o values, respectively.

[b]The x_i and y_i values were changed in increments of r = 0.001 over $-0.01 < r < 0.01$ for $L_s < 230°$; for all other values, the x_i and y_i values were changed in increments of r = 0.005 over $-0.05 < r < 0.05$.

[c]The $(r - r_i)^2$ value is lower than for $x_i = -0.004$, $y_i = 0.011$ meaning this value is probably gives a minimum $(r - r_i)^2$ value.

[d]Dust covered a small portion of the SPC preventing measurements at 240–270° W.

[e]Dust covered a small portion of the SPC preventing measurements at 255–270° W.

Table IV. Mean x_o, y_o, and center of the SPC based on measurements made between 1956 and 2018; the sample standard deviations for the mean x_o and y_o values are in parentheses. The number of values is n.

L_s range	Mean x_o	Mean y_o	n	SPC center
180.1°–230°	–0.0043 (0.0054)	0.0029 (0.0064)	47	56° W, 89° S
230.1°–250°	–0.013 (0.013)	0.020 (0.015)	37	32° W, 87° S
250.1°–270°	–0.022 (0.011)	0.046 (0.0093)	24	26° W, 84° S
270.1°–290°	–0.013 (0.012)	0.038 (0.013)	18	19° W, 85° S
290.1°–310°	–0.0077 (0.0096)	0.022 (0.014)	7	20° W, 87° S

Table V. Summary of early spring (L_s < 230°) SPC data 1798–2018 compared to the 1999 results (James et al. 2001)

Apparition	Statistical difference[a]	Mean difference in SPC radius (°)[b]	Number of values	Reference
1798	No	0.41[c]	5	Slipher (1962), Fig. 5
1892	No	0.77[c]	11	Barnard (1903)
1894	Yes	1.05[c]	5	Barnard (1903)
1907	No	–0.60[c]	6	Iwasaki et al. (1986a)
1909	No	0.46[c]	11	Slipher (1962), Fig. 5
1924	Yes	1.79[c, d]	11	Slipher (1962), Fig. 4
1924	Yes	2.44[c]	5	Iwasaki et al. (1986a)
1939	No	0.25[c]	6	Iwasaki et al. (1986a)
1954	Yes	–2.10[c]	6	Iwasaki et al. (1986a)
1956	No	–0.02[c]	6	Dollfus (1965)
1956	–	–0.32	4	Iwasaki et al. (1986a)
1969	–	–0.26[e]	2	Collins (1971)
1971	Yes	–0.96	14	Iwasaki et al. (1986a)
1977	No	–0.72	7	James & Lumme (1982)
1986	Yes	–1.17	11	James et al. (1990)
1986	–	–0.70	3	Iwasaki et al. (1989)
1988	–	–0.61	1	Iwasaki et al. (1990)
1988	Yes	3.93	1	Beish et al. (1991)
1988	–	0.06	4	McKim (1991)[f]
2003	Yes	–0.87	8	McKim (2010b)[f]
2003	Yes	–0.89	10	Current work
2018	No	–0.01	11	Current work

[a]Based on a two-tailed Wilcoxon signed-rank test at the 95 % confidence level used in this study.
[b]The mean difference in SPC radius is the 1999 radius minus the radius at the given apparition.
[c]Individual measurements were used; in other cases, mean values of several measurements were used.
[d]Slipher photographic measurements are not included since these were undoubtedly covered in the work by Iwasaki et al. (1986).
[e]Based on my analysis of far-encounter Mariner 7 images made in August 1969 as published in Collins (1971).
[f]Only mean latitudes based on 40 or more measurements are included.

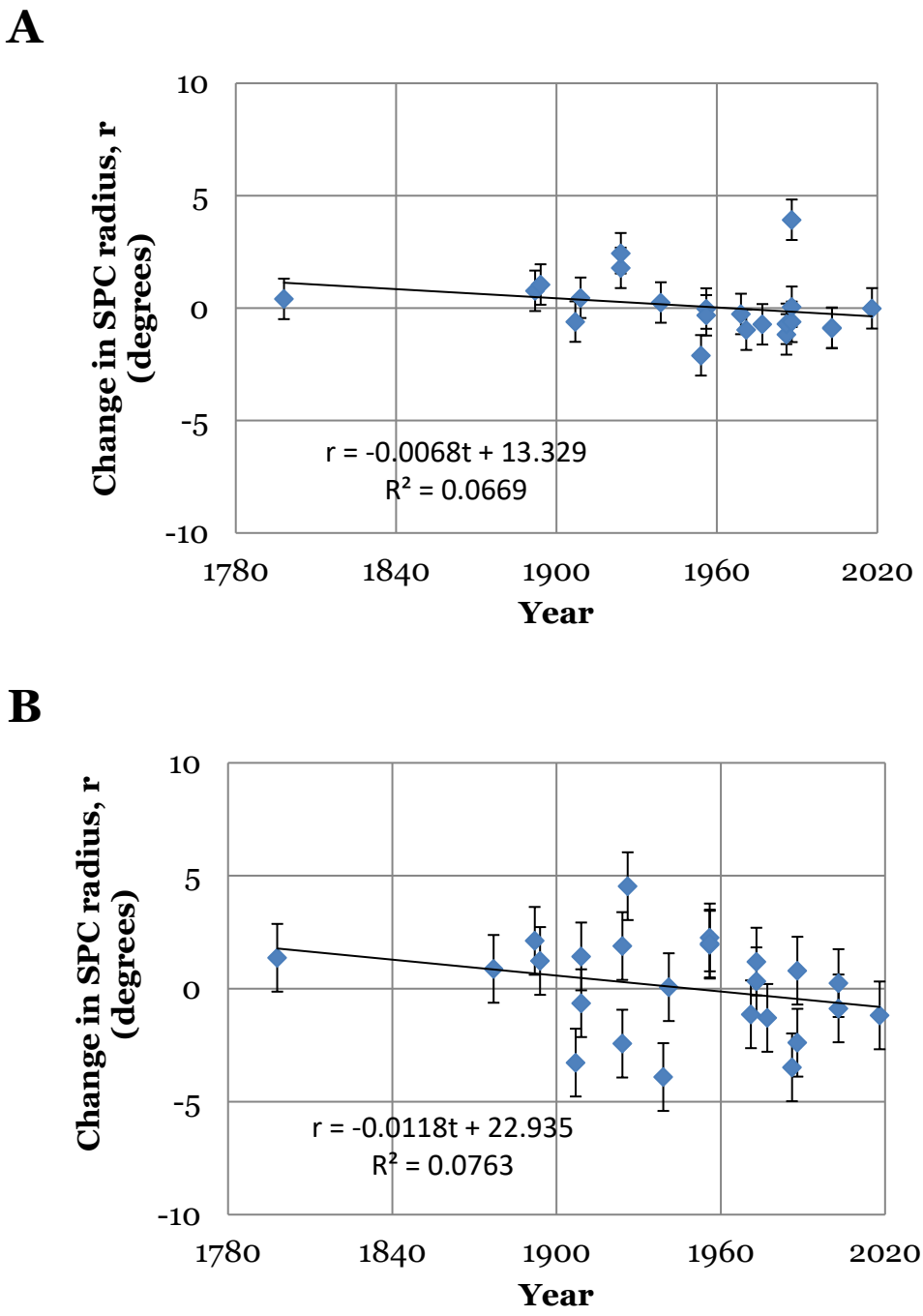

Figure 2. Mean difference in SPC radius (1999 – yearly value) versus the year for the top graph, **A** (L_s < 230°) and the bottom graph, **B** (L_s > 230°). Most years had several SPC radii at different L_s increments and, hence, a mean difference could be evaluated. Estimated uncertainties are 0.9° and 1.5° for Figures 2A and 2B.

The writer measured the SPC boundaries from Fischbacher et al. (1969). The mean radii, with standard deviations in parentheses, are 32.2° (1.6°), 30.5° (1.2°), 29.0° (0.3°), 26.3° (1.6°), and 21.7° (0.8°) for L_s = 190°, 200°, 210°, 220°, and 230°, respectively. The SPC boundaries at different longitudes were fitted to the three parameter model

summarized in James and Lumme (1982) and Iwasaki et al. (1986b). The mean SPC center for L_s = 190°–230° is 56° W, 88° S. This is close to the results in Table IV. Therefore, the writer concludes the center of the shrinking SPC for L_s = 190°–230° has not shifted much in the last century. The mean discrepancy, 1999 (James et al. 2001) minus Fischbacher et al. (1969), is –1.18°.

Beish (2012) reports mean SPC radii for six different apparitions between 1986 and 2005. The mean value of the 1999 (James et al., 2001) minus Beish (2012) radii for L_s = 200°–230° is 2.35°.

After L_s = 230°

The SPC continues to shrink after L_s = 230°, but the cryptic terrain (Kieffer et al. 2000) complicates the interpretation of results. This is because the SPC is less circular and is centered farther from the South Pole. Therefore, once the cap edge reaches the edge of the cryptic terrain, the cap boundary near 210° W shifts rapidly to the south. This is evident in Table IV. Measurements carried out between 1798 and 2018 are compared to those made by spacecraft in 1999 (James et al. 2001). The results are summarized in Table VI. One trend is the mean discrepancy between each of the values and the 1999 radii is 0.07° with a standard deviation of 2.09°. The corresponding values before L_s = 230° are 0.09° and 1.32°. Therefore, the mean discrepancy between the SPC and 1999 SPC radii (James et al. 2001) during early and late spring is small.

There is some scatter in the late spring SPC results. Mean discrepancies in SPC radii compared to 1999 range from –3.91° (1939) to 4.54° (1926). This range is larger than the corresponding one for early spring (Table V). This may be caused by the cryptic terrain, and the fact that not all longitudes were considered in some SPC studies.

Once again, the mean SPC discrepancies compared to 1999 were plotted against the year. A mean uncertainty of 1.5° was estimated for all points based on a combination of several factors. The results are shown in Figure 2B and are fitted to a best-fit line. The correlation coefficient (r) equals 0.2762. Based on a *t* test, the correlation is not statistically significant. This, along with the negligible mean difference between the SPC radii summarized in Tables V and VI compared to 1999 SPC radii, leads the writer to conclude the SPC has not underwent large, long-term size changes in the last 125 years.

Measurements of the SPC maps reported in Fischbacher et al. (1969) were analyzed and the resulting cap sizes and locations of the cap center were computed. The mean cap radii, with standard deviations in parentheses, are 17.0° (3.5°), 12.3° (4.0°), 8.9° (3.1°), and 6.3° (3.4°) for L_s = 240°, 250°, 260°, and 270°, respectively. The mean discrepancy, 1999 radii minus Fischbacher et al (1969) radii, is +0.005 planetary radii or +0.6 degrees of latitude. The positions of the SPC center, based on maps in Fischbacher et al. (1969), are all close to each other with a mean of 25° W, 85.6° S. This is similar to those in Table IV.

Beish (2012) reports mean SPC radii for six different apparitions between 1986 and 2005. The mean value of 1999 (James et al. 2001) minus Beish (2012) SPC radii for L_s = 235°–275° is 0.87°.

It is difficult to estimate the uncertainty of the images used in this study. Therefore, a sample of the data was examined. The mean telescope size used for L_s = 210-214° in 2018 was 0.37 m which is consistent with a theoretical resolution of 0.31 arcsec (Dobbins et al. 1988, p. 7). This corresponds to a resolution of over one degree of latitude for the SPC. The standard error of estimate of the values in Figures 2A and 2B, with respect to the

linear equations listed, are 1.3° and 2.1° of SPC latitude, respectively (Larson and Farber 2006). The mean uncertainty of SPC radii for 2003, 2005, and 2018 is 0.6° for L_s < 230° and is 1.0° for L_s > 230°. The uncertainties do not change much as the cap size decreases for L_s = 186° to L_s = 230°. They decrease with cap size a little after L_s > 230°. The mean percent error for L_s < 230° and L_s > 230° are 2.3 % and 8.8 %, respectively. Based on these results along with those in Figure 2, it is concluded the SPC has maintained nearly the same size to within 3 % and 10 % for L_s < 230° and L_s = 230°–270°, respectively.

Table VI. Summary of late spring (L_s > 230°) SPC data 1798–2018 compared to the 1999 results (James et al. 2001). In the apparitions before 1956, individual SPC radii were compared to the 1999 SPC radii. Although this is less accurate, the data are believed to be extensive enough to have covered many longitudes. Beer and Madler report SPC radii for 1830; however, only three points could be compared to the 1999 radii and hence these are not listed. The 1830 radii were 3.8° smaller than the 1999 radii at the corresponding L_s value.

Apparition	Statistical difference[a]	Mean difference in SPC radius (°)[b]	Number of values	Reference
1798	–	1.37	7	Schröter cited in Slipher (1962)
1877	–	0.88	8	Schiaparelli cited in Slipher (1962)
1892	Yes	2.12	23	Barnard (1895, 1903)
1894	No	1.23	11	Barnard (1895, 1903)
1907	–	–3.27	1	Iwasaki et al (1986a)
1909	–	–0.64	4	Iwasaki et al (1986a)
1909	–	1.43	12	Lowell & Slipher cited in Slipher (1962)
1924	–	–2.43	4	Iwasaki et al (1986a)
1924	–	1.89	12	Measured from Slipher (1962)
1926	–	4.54	5	Iwasaki et al (1986a)
1939	–	–3.91	4	Iwasaki et al (1986a)
1941	–	0.07	4	Iwasaki et al (1986a)
1956	–	1.95	4	Iwasaki et al (1986a)
1956	–	2.27	4	James & Lumme (1982)
1956	Yes	2.00	10	James et al. (1987)
1971	Yes	–1.13	15	James and Lumme (1982)
1973	–	0.33	4	James and Lumme (1982)
1973	–	1.20	4	Iwasaki et al. (1986b)
1977	Yes	–1.29	5	James and Lumme (1982)
1986	–	–3.48	3	Iwasaki et al. (1989)
1988	Yes	–2.39	6	Iwasaki et al. (1990)
1988	Yes	0.80	10	McKim (1991)[c]
2003	No	0.25	7	McKim (2010b)[c]
2003	Yes	–0.87	12	Schmude (2017) & Current work
2018	Yes	–1.18	5	Current work

[a]See footnote *a* in Table V.
[b]See footnote *b* in Table V.
[c]Only mean latitudes based on 40 or more measurements are included.

SPC Irregularities

Irregular features (projections and isolated bright spots) develop near the edge of the SPC as it shrinks. These may be used to search for year-to-year changes in the SPC. Table VII lists a few of them. All features in this table were imaged in 2018 except for Thyle Collis. One new feature—the ice-filled crater Secchi—was imaged as a bright projection in 2018 by A. Elia on May 28, 2018; see the ALPO Japan Latest Mars website at alpo-j.asahikawa-med.ac.jp/Latest/index.html and go to the Mars section and to May 28, 2018. This feature was previously imaged in Mars Global Surveyor images (James et al. 2001).

Table VII. Irregularities near or on the edge of the shrinking south polar cap (SPC)

	Location				
L_s	°W	°S	Name	Description	Source
173–190	258	58	Crater Secchi	Isolated bright spot	James et al. (2001) & Batson et al (1979)
206–214	30	65	Mons Argentis	Bright spot in SPC	Schmude et al. (2004) & Schmude (2017)
214–253	30	68	Mons Argentis	Double projection	Schmude et al. (2004) & Schmude (2017)
253–261	30	76	Mons Argentis	Single projection	Schmude et al. (2004) & Schmude (2017)
213–253	159	65	Thyles Mons	SPC projection	Schmude et al. (2004)
253–261	150	73	Thyles Mons	Isolated bright spot	Slipher (1962) & Schmude et al (2004)
218–220	225	72	Thyles Collis	Isolated bright spot	Veverka & Goguen (1973) & James et al. (2001)
238–256	319	72	Novus Mons[a]	SPC projection	Antoniadi (1975), Schmude et al. (2004) & Schmude (2017)
256–274	319	75	Novus Mons[a]	Isolated bright spot	Schmude et al. (2004)

[a]Also called the Mountains of Mitchel

Mariner 6 and 7 far-encounter images (Collins 1971) were measured. Stonyhurst grids were used in the analysis. Small, white, north-pointing projections at the SPC edge were measured to be at 123° W, 170° W, and 231° W near L_s = 200°. The one at 123° W may have been imaged on June 26, 2018 by B. MacDonald; see the ALPO Japan Latest website at alpo-j.asahikawa-med.ac.jp/Latest/index.html and select Mars and the appropriate date. The mean SPC latitude was also evaluated and is included in Table V.

A planet-encircling dust storm developed in mid-2018. Dust clouds covered portions of the SPC, which undoubtedly affected Novus Mons' sublimation rate. According to the dust model of Bonev et al. (2002), bright areas, like Novus Mons, should shrink faster in the presence of a dust storm. Figure 3 illustrates two images of Novus Mons taken at nearly the same seasonal date. Longitude and latitude values of Novus Mons were measured for both images using WinJUPOS. Novus Mons had an area at least 30 % larger

in 2003 (when there was no planet encircling dust storm) than in 2018 (during a planet-encircling dust storm). Therefore, this result supports the model of Bonev et al. (2002).

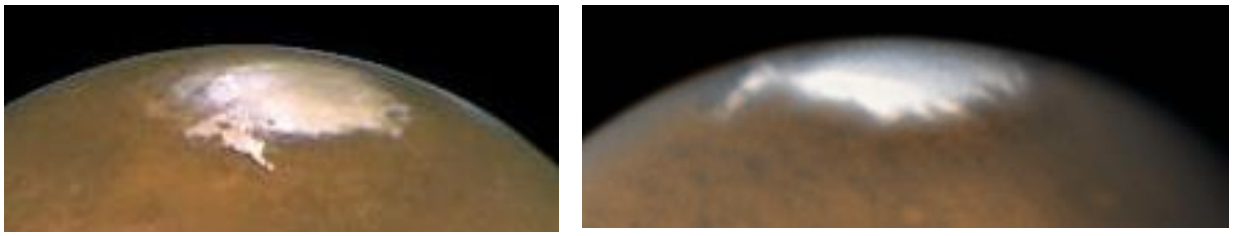

A **B**

Figure 3. Images of Mars showing Novus Mons at nearly the same seasonal date in 2003 and 2018. **A** August 26, 2003 (about 23:46 UT) by the Hubble Space Telescope, Credit: NASA, J. Bell (Cornell U.) and M. Wolff (SSI) [NASA/JPL/Space Science Institute], **B** September 8, 2018 (23:38.9 UT) by D. Peach. Both images were taken near L_s = 247°.

Cryptic Terrain

The cryptic terrain is a name given to a large dark area, which develops inside the SPC during early spring (Kieffer et al. 2000). It begins to darken near L_s = 198° and remains dark thereafter (James et al. 2001). The SPC boundary reaches the northern edge of the cryptic terrain in late spring (Kieffer 1979). After this, the cap center appears to shift several degrees from the pole (James et al. 2001). Titus and Kieffer (2002) report maps of the shrinking SPC in 1999 and 2001 based on 30 μm temperature measurements. (Infrared light with a wavelength of 30 μm may be used to measure surface temperatures.) Essentially, they determined the temperatures of different parts of the SPR using these data. Frozen carbon dioxide ice is much colder than bare ground and, hence, this technique can distinguish between dark ice and bare ground. Therefore, they were able to determine where the CO_2 ice was including dark ice.

What is the cryptic terrain? Kieffer et al. (2000) reports it remains at nearly the same temperature as the nearby dry ice cap at L_s ~ 219°. They report it has a larger grain size than the surrounding cap, and that it may even be a slab of ice. A thin coating of frost may cover it in winter and would sublime during the early spring leaving a dark area. Alternatively, the cryptic terrain may have developed when a dust storm deposited dark material onto the SPC, which became embedded in the SPC (see the acknowledgements).

How long does the ice remain in the cryptic terrain? The writer of this paper measured the mean size of the shrinking SPC from the thermal maps reported in Titus and Kieffer (2002) for L_s = 200°–250°. The difference in mean SPC radii between the 1999 optical radii (James et al. 2001) and the thermal radii (Titus and Kieffer 2002) for 1999 was 0.09°, with an estimated uncertainty of 1°. Therefore, it is concluded the difference in SPC radii between thermal and visible light images was negligible in 1999. There was also a negligible difference between the visible light images in 1999 at L_s = 247.5° (James and Lumme 1982) and the thermal results in 2001 (Titus and Kieffer 2002). Therefore, the area covering the cryptic terrain was about as cold as dry ice at L_s ~219° in 1999, but several weeks later at L_s ~ 250° it had warmed up to the temperature of bare ground.

The cryptic terrain was also imaged in 2018. See Figure 4. The writer measured its northern boundary from several 2018 images made over L_s = 218°–220°. The mean

northern boundary was 73° S for 180°–210° W and 76° S for 210°–270° W. Later on, at L_s = 232°–237°, its mean boundary was at 75° S and 77° S for 180°–210° W and 210°–270° W, respectively. These results are consistent with those reported elsewhere (Kieffer et al. 2000; James et al. 2001) and are similar to the boundary in a drawing of Depressio Magna in Figure 135 in Antoniadi (1975). Therefore, it is concluded the cryptic terrain was imaged in 2018 and is the same feature as Depressio Magna in Figure 135 in Antoniadi (1975).

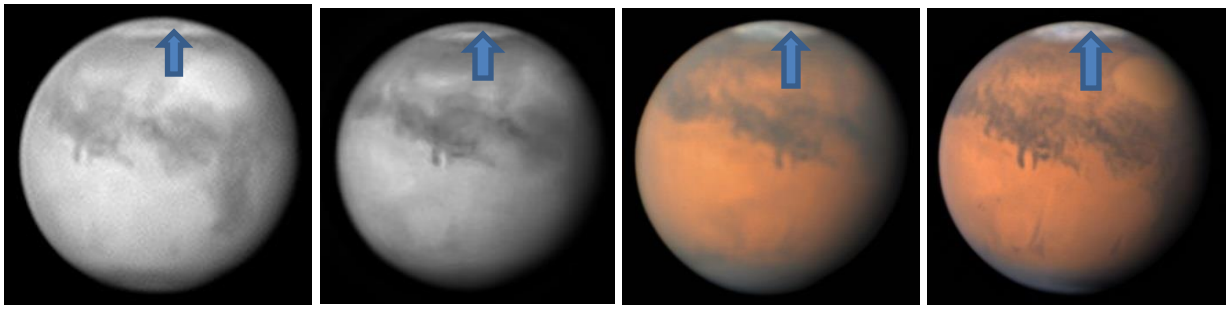

A **B** **C** **D**

Figure 4. Images of the cryptic terrain (arrows) taken in late August 2018 (L_s = 232°–237°). All images show south at the top. **A**: August 14 (23:55.2 UT) by C. Pellier, IR filter; **B**: August 23 (3:24.7 UT) by G. Walker, IR filter; **C**: August 26 (3:59.4 UT) by D. Peach; **D**: August 27 (6:25.1 UT) by D. Peach.

Others have also drawn the cryptic terrain in previous apparitions. See Table VIII. The appearance of the cryptic terrain probably depends on the imaging technique used along with the seeing conditions. It appears narrow because of foreshortening. It is a resolved feature in many images, but poor seeing and small apertures may prevent this feature from being resolved. In several images (Figures 4A, 4B, and 4D), there is a long east to west dark feature, which may be Rima Australis.

South Polar Hood

The software package WinJUPOS was used along with mostly RGB or green filter images made between 2001 and 2018 to measure the northerly extent of the SPH (Schmude 2019). Since Mars is close to the Earth for only a few months each apparition, several apparitions are needed to study the SPH from late Martian summer through early spring of the next Mars year. There are five main conclusions of this and other studies (Benson et al. 2010; Wang and Ingersoll 2002; Schmude 2018b). Firstly, the SPH starts developing in late summer (L_s ~330°). Secondly, it is fully developed in early autumn at around L_s = 20°. The Hellas basin begins to brighten during autumn, and it is difficult to distinguish it from the SPH after this time is a third conclusion. Fourthly, the SPH is less brilliant than the NPH. A final conclusion is the mean northern boundaries of the SPH, in °S, for L_s = 20°–80° and L_s = 100°–160° at local times of 9h to 16h, are 37.4, 40.0, 41.2, 42.7, 44.0, 44.2, 44.6, and 43.6, respectively.

Other White Clouds

For the sake of completeness of this review, white cloud observations and summaries made by others are examined. The writer plans to carry out a study of white clouds in a separate study.

Table VIII. Previous drawings or images of the cryptic terrain

Date or year	Observer	Source
July 21, 1845	Mitchel	Barnard (1895) p. 438
July/Aug. 1892	Barnard	Barnard (1895), Barnard (1903)
July 2 & 8, 1894	Barnard	Barnard (1903)
1909	Fournier	Antoniadi (1975), p. 299
Aug. 7, 1924	Antoniadi	Antoniadi (1975), p. 324, plate 8
Mid 1969	Mariner 7	Collins (1971)
June 4, 1971	Dragesco	Collinson (1973) Fig. 7
May 28, 1986	Beish	McKim (1989), Fig. 8
July 18, 1986	Miyazaki	McKim (1989), Fig. 7
July 23, 1986	Minami	McKim (1989), Fig. 6
June 22, 1988	Schmude	Schmude (1989), Fig. 3C
July 19, 1988	McKim	McKim (1991), Fig. 2C
July 1-5, 2003	Parker	Schmude (2004), Fig. 1
May 27, 2005	Adachi	Schmude (2017), Fig. 1B
2018	Many	Current work

Martian white clouds have been observed for over a century (Slipher 1962; De Vaucouleurs 1954). De Vaucouleurs (1969) reported clouds covering surface details are rare except for polar hoods. More recently, Beish and Parker (1990) carried out a study of different kinds of Martian clouds based on 9,650 visual and photographic observations made between 1969 and 1984. They report clouds in the SPR are less frequent than in the NPR. This trend is consistent with the study carried out by Smith (2004). Essentially, Smith concludes Mars' atmosphere has less water ice and more dust for L_s = 180°–360° (southern spring and summer) than during L_s = 0°–180° (southern autumn and winter). More recently, Beish (2012) expanded his study to include 24,130 observations made between 1965 and 1995. He reports water ice cloud activity and surface fogs are more common in the Northern Hemisphere during spring and summer than in the Southern Hemisphere during those seasons. McKim (1984, 1985, 1987, 1989, 1991, 1992, 1995, 2005, 2006, 2007, 2009, 2010b) has summarized observations of white clouds seen near or within the SPR on a month-by-month basis for 1980–2004. The writer, R. Schmude, Jr., has broken down McKim's summaries into clouds seen on different parts of Mars' disk during spring and summer. He only counted clouds near or within the SPR. The L_s values are for the middle date of each month and are from https://ssd.jpl.nasa.gov/horizons.cgi. Over 300 months of cloud data were compiled. The breakdown is 24 % lie on the morning limb, almost 23 % lie on the morning terminator, 16 % lie on the afternoon limb, 14 % lie on the afternoon terminator, and 23 % lie away from disk edges. The results for different areas are summarized in Table IX. Isolated SPR clouds away from disk edges were most often reported in Ausonia (44° S, 245° W), Eridania (45° S, 213° W), and Hellas (45° S, 295° W). De Vaucouleurs (1969) reported observing a large-whitish cloud system on June 25, 1937 (L_s = 171°), over the Thaethontis-Electris-Atlantis region. A white cloud in Phaethontis and Electris was imaged on December 1, 2007, at 4:33 UT by D. Parker (Venable 2018; Fig. 40). Kuiper (1957) also reported a dense cloud cap developing between September 6 and 9, 1956 (L_s = 261°–262°).

Table IX. Summary of white clouds observed in the SPR during the spring and summer; all data are based on the Mars reports by McKim covering 1980–2004. Key: blank–not reported; 1- reported less than one third of the time; 2- reported between one-third and up to two-thirds of the time; 3- reported at least two-thirds of the time. On rare occasions, clouds were reported in Argyre II, Dia, Icaria, Mare Australe, and Phaethontis. Hellas is not included.

	L_s in degrees (Morning limb/terminator)							
Feature	**180–202.5**	**202.5–225**	**225–247.5**	**247.5–270**	**270–292.5**	**292.5–315**	**315–337.5**	**337.5–360**
Argyre	1	1	1	1	1	2	3	2
Ausonia		1	2	2	1	1	1	1
Electris		1	3	1	1	1	2	
Eridania		2	2	2	2	1	3	1
Hellaspontus			1					1
Noachis	1	2		1	1	1	2	
Phaethontis		2	2	1	1	2	2	1
Thaumasia			2	1	1	1	1	1
Yanos Region					1			1
	L_s in degrees (Afternoon limb/terminator)							
Feature	**180–202.5**	**202.5–225**	**225–247.5**	**247.5–270**	**270–292.5**	**292.5–315**	**315–337.5**	**337.5–360**
Argyre		1	2	2	2	3	1	2
Ausonia			2	2	2	1	1	1
Electris		2		1				
Eridania	1			1	1		2	1
Noachis			2	1				1
Phaethontis		2	2	1	1	2	2	1
Thaumasia			2	1	1	1	1	1
	L_s in degrees (away from limbs)							
Feature	**180–202.5**	**202.5–225**	**225–247.5**	**247.5–270**	**270–292.5**	**292.5–315**	**315–337.5**	**337.5–360**
Argyre	1	1			1			
Ausonia								2
Electris		1						1
Eridania	1		1					2
Novus Mons					1			
Thyle I				1	1			
Thyle II				1	1			

Dust Activity

Dust activity in the SPR was reported in 35 apparitions between 1880 and 2018 (McKim 1999, 2006, 2007, 2009, 2010a, 2011, 2012, 2018; Schmude 2002, 2019; Schmude et al. 2004; Venable 2018). This represents 53 % of the apparitions during that time. Furthermore, astronomers only observe Mars for part of each apparition and, consequently, many SPR dust storms have probably gone undetected. Therefore, the

writer of this paper believes dust activity is common in the SPR. Dust may interfere with SPC measurements in two ways: deposited dust, on the SPC, darkens the ice which may lead to an underestimation in cap size (Schmude 2018a) and dust clouds may obscure the SPC edge. This happened in 2018. See Figure 1B. The writer believes dust has led to some of the scatter in SPC size measurements.

Dust may have also enhanced craters. During mid-2018, over a dozen bright circular features were imaged. Each one was ~100 to ~300 km across. Most of these match up with known craters (Batson et al. 1979). Apparently, there was either suspended dust in these craters or a brighter layer of dust was deposited on the crater floors. To the best of my knowledge, this has not been imaged from Earth before. A list of these is given in Table X. Milika-Nicholas imaged a ~100 km crater on September 29, 2018. Interestingly, this was imaged in the bright desert area of Mars. The crater probably appeared bright because of dust. Figure 5 shows an image with bright craters (see arrows).

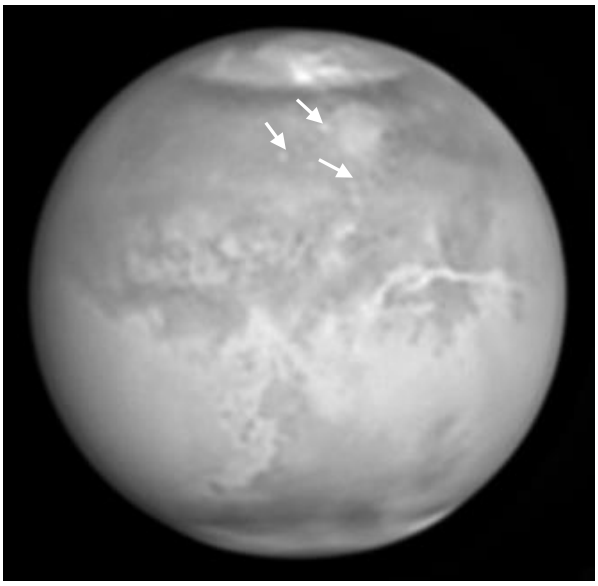

Figure 5. This image shows bright circular regions, which correspond to craters. South is at the top. **A** July 19, 2018 (16:27.8 UT) by A. Wesley, near infrared.

Bright, dusty craters have apparently been imaged from spacecraft and the Hubble Space Telescope. Mariner 9 imaged the 60 km crater labeled "Km" at 64° W, 16° S near Valles Marineris (Batson and Bridges 1979; image P1A02998.tif at the NASA Photojournal website) along with the bright Valles Marineris canyon system. Several craters near Argyre appear brighter than the surrounding terrain in JPL Mosaic 211-53040 (Strom et al. 1992, p. 387). More recently, the Hubble Space Telescope imaged Mars on July 18, 2018. This image shows several bright craters including Argyre, Galle, Helmholtz, Green, and Lohse (Hubblesite). Several bright craters including Argyre, Galle, Hale, Bond, Lohse, and Darwin were bright in July and August of 2018 (Malin et al. 2018a, b).

Table X. Bright areas, which correspond to craters imaged in 2018. The mean longitudes and latitudes are those measured from images and lie close to large craters listed elsewhere (Batson et al. 1979). In a few cases, the two-letter abbreviations in Batson et al. (1979) are used. The mean longitude and latitude values have an uncertainty of about one degree.

	Mean values	
Crater name	**Longitude (°W)**	**Latitude (°S)**
Green	10	52
Lohse	17	43
Darwin	22	52
Helmholtz	22	45
Ks	26	41
Wirtz	27	48
Galle	32	51
Ng	33	44
Maraldi	34	62
Bond	37	32
Hale	37	35
Lowell	84	52
Newton	156	42
Schaeberle	309	24
Ej	323	19
Lv	326	37
Schiaparelli	344	2

SPC Size on the Morning and Afternoon Terminator

There may be a correlation between the L_s value of the opposition date and the mean difference in SPC radius (compared to 1999) in Tables V and VI. This is because the SPC borders the afternoon terminator before opposition and borders the morning terminator after opposition. Therefore, if opposition takes place in early Martian spring, most of the SPC measurements would be made after opposition and, hence, the SPC would be next to the cold morning terminator. The opposite is true if opposition takes place in early Martian summer. Two graphs were constructed. One shows the mean difference (1999 radius – SPC radius for a given apparition) versus the L_s value on opposition day. In this graph, only early spring SPC radii differences ($L_s < 230°$) are used. Figure 6A shows the results. For example, opposition occurred on July 27, 2018, and $L_s = 219°$ (Astronomical Almanac). Therefore, the point $L_s = 219°$, –0.01° would be plotted. A similar graph shows results for late spring SPC ($L_s > 230°$). See Figure 6B. In both Figures 6A and 6B, the mean radii difference becomes more positive as L_s on opposition date increases. This is consistent with the SPC appearing smaller when it borders the afternoon terminator than when it borders the morning terminator. The correlation coefficients for these graphs are 0.4837 and 0.6001 for $L_s < 230°$ and $L_s > 230°$, respectively. A *t* test was carried out on the two correlation coefficients at the 95 % confidence level (Larson and Farber 2006). Both correlation coefficients are statistically significant.

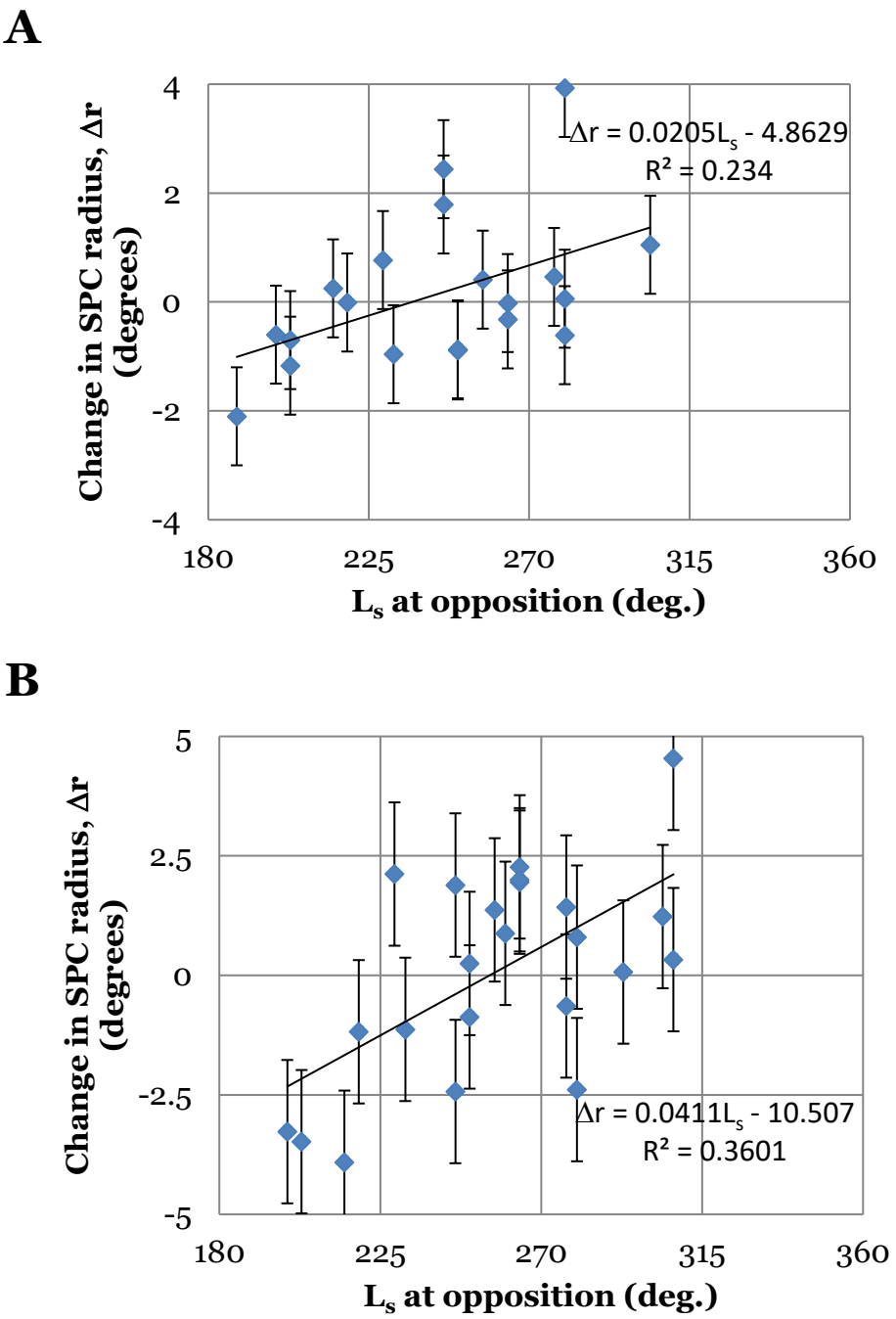

Figure 6. Graphs of the difference in SPC radius (1999 – year value) versus the areocentric longitude of Mars on the opposition date. Graph **A** shows the mean difference in early spring (L_s < 230°) and graph **B** shows the mean difference in late spring (L_s > 230°). Errors are the mean standard error of the estimate. Uncertainties are the same as in Figure 2.

One explanation for the trends in Figures 6A and 6B is that ground frost and condensate clouds forming during the coldest part of the Martian day may eliminate phase darkening and may extend beyond the edge of the SPC. Dobbins et al. (1988, p. 72) report ground frost can be distinguished from condensate clouds with the use of filters. Ground frost is brighter in a green filter than a blue one whereas the reverse is the case

for condensate clouds. This will lead to a larger size measurement than if phase darkening is present. Afternoon dust may also cause the SPC to appear smaller than what it is.

DISCUSSION

About 53 % and 80 % of the SPC measurements in Tables V and VI, respectively, have statistical differences compared to the 1999 radii based on the Wilcoxon signed-rank test (Larson and Farber 2006). Much of this difference may be caused by the discrepancy between when the SPC is on the morning and afternoon terminators. Additionally, the shape and position of the SPC in late spring may lead to additional scatter.

The results in Figures 2A and 2B show that there are no long-term growth or shrinkage trends in the SPC over the last 125 years (or MY = –33 to MY = 34). This is consistent with there being almost no change in SPC size during 1999–2003 or MY = 24–26 (Benson and James 2005). There is some evidence that suggests the SPC has followed nearly the same regression trend over the last ~350 years. The drawing by Huygens on August 13, 1672 ,or MY = –150 (Flammarion 2015), is consistent with the SPC shrinking faster near 210° W than near 30° W. This is consistent with modern observations (James et al. 2001). During the eighteenth century, Maraldi and Herschel each noted the SPC was not centered at the South Pole in 1719, or MY = –125, and 1783, or MY = –91, respectively (McKim 1999; Herschel 1784). Once again, this is consistent with modern observations (James et al. 2001).

Four questions were posed at the beginning of this review. Updated answers are now given. The size measurements and appearance of the early spring SPC are consistent with it displaying a nearly consistent behavior over at least the last 125 years. Differences in SPC size, as summarized in Tables V and VI, are apparently the result of the cap appearing larger on the morning terminator than on the afternoon terminator. Regarding the third question, astronomers have observed the cryptic terrain since at least 1845. In 2018, it had nearly the same southern boundary as Depressio Magna, which Antoniadi (1975) reports in his Figure 135, and the dark areas imaged by the Mars Global Surveyor (James et al. 2001). The nature and frequency of white clouds in the SPR, raised in the fourth question is more uncertain. It is unlikely large annular clouds, similar to those which form in the north polar region (Schmude 2018c), form in the SPR. The general trend is that white clouds occur less frequently in the SPR than in the NPR.

ACKNOWLEDGEMENTS

The writer would like to thank the individual at the 2018-GRAM meeting who suggested a large dust storm deposited dust, which is a possible cause of the cryptic terrain.

REFERENCES

ALPO Japan Mars Latest at alpo-j.asahikawa-med.ac.jp/Latest/index.html.

Antoniadi, E.M. 1975. The Planet Mars. Translated by Patrick Moore, Keith Reid Ltd. Shaldon, D. Mars-exploration.co.uk/docs/Antoniadi-The%20Planet%20Mars-1930.pdf.

Astronomical Almanac, U. S. Govt. Printing Office, Washington D.C.

Barnard, E.E. 1895. Micrometrical measures of the diameters of the south polar caps of Mars in 1892 and 1894 with the 12-in and 36-in refractors and on the diameter and

polar compression of the planet. Popular Astronomy, 2(10), 433–443. adsabs.harvard .edu/full/1895PA.....2..433B.
Barnard, E.E. 1903. The south polar cap of Mars. The Astrophysical Journal, 17, 249–258. adsabs.harvard.edu/full/1903ApJ....17..249B.
Batson, R.M., P.M. Bridges, and J.L. Inge. 1979. Atlas of Mars. NASA, Washington DC. https://catalog.hathitrust.org/Record/000700307.
Beish, J.D. 2012. Observing the Planet Mars. Unpublished manuscript. (For the latest edition go to alpo-astronomy.org, click on "Mars Section" and then click on "Mars Observer's Café").
Beish, J.D. and D.C. Parker. 1990. Meteorological survey of Mars, 1969-1984. J. Geophys. Res., 95, 14,657–14,675. https://doi.org/10.1029/JB095iB09p14657.
Beish, J.D., D.C. Parker, C. Hernandez, D. Troiani, and H. Cralle. 1991. The International Mars Patrol in 1987-1988—Part I. Journal of the Association of Lunar and Planetary Observers, 35(1) 4–13. alpo-astronomy.org.
Benson, J.L., and P.B. James. 2005. Yearly comparisons of the martian polar caps: 1999–2003 Mars Orbiter Camera observations. Icarus, 174, 513–523. doi:10.1016/j.icarus .2004.08.025.
Benson, J.L., D.M. Kass, A. Kleinböhl, D.J. McCleese, J.T. Schofield, and F.W. Taylor. 2010. Mars south polar hood as observed by the Mars Climate Sounder. J. Geophys. Res., 115, E12015, doi:10.1029/2009JE003554.
Bonev, B.P., P.B. James, J.E. Bjorkman, and M.J. Wolff. 2002. Regression of the Mountains of Mitchel polar ice after the onset of a global dust storm on Mars. J. Geophys,. Res. 29(21) https://agupubs.onlinelibrary.wiley.com/doi/full/10.1029 /2002GL015458.
Collins, S.A. 1971. The Mariner 6 and 7 Pictures of Mars. NASA SP–263, Washington DC. https://www.scribd.com/document/45904461/The-Mariner-6-and-7-Pictures-of-Mars.
Collinson, E.H. 1973. Section Report: Mars in 1971. J. Brit. Astron. Assoc. 83, 283–290. adsabs.harvard.edu/full/1973JBAA...83..283C.
de Vaucouleurs, G. 1954. Physics of the Planet Mars. Faber & Faber, Ltd. London.
de Vaucouleurs, G. 1969. Cloud Activity of Mars Near the Equinox: Comparison of the 1937 and 1969 Oppositions. Planetary Atmospheres, proceedings from the 40th IAU Symposium held in Marfa, TX, Oct. 26-31. Edited by C. Sagan, T. C. Owen and H. J. Smith, International Astronomical Union Symposium No. 40, Dordrecht Reidel, 310–319.https://link.springer.com/chapter /10.1007/978-94-010-3063-2_40.
Dick, T. 1838. Celestial Scenery; or, The wonders of the Planetary System Displayed; illustrating the Perfections of Deity and a Plurality of Worlds. E. and L. Merriam, Brookfield, MA. https://catalog.hathitrust.org/Record/011631524.
Dobbins, T.A., D.C. Parker, and C.F. Capen. 1988. Introduction to Observing and Photographing the Solar System. Willmann–Bell, Inc. Richmond, VA. https://www .willbell.com/ccd/CCD3.HTM.
Dollfus A. 1965. Étude de la planète Mars de 1954 A 1958. Annales D'Astrophysique, 28, 722-747. adsabs.harvard.edu/full/1965AnAp...28..722D
Fischbacher, G.E., L.J. Martin, and W.A. Baum. 1969. Martian Polar Cap Boundaries Final Report, Part A. Planetary Research Center, Lowell Observatory, Flagstaff, AZ.
Flammarion, C. 2015. Camille Flammarion's the Planet Mars. (translated by P. Moore and edited by W. Sheehan) Springer, New York. https://www.springer.com/us/book /9783319096407.

Hahn, G.H. 2019. See: Jupos.privat.t-online.de/index.htm.

Herschel, W. 1784. On the remarkable Appearances at the Polar Regions of the Planet Mars, the Inclination of its Axis, the Position of its Poles, and its spheroidical Figure; with a few Hints relating to its real Diameter and Atmosphere. Philosophical Transactions LXXIV, 233–277.https://royalsocietypublishing.org/doi/pdf/10.1098/rstl.1784.0020.

Hubblesite at https://hubblesite.org/image/4215/gallery.

Iwasaki, K., Y. Saito, and T. Akabane. 1986a. "Interannual Differences in the Regression of the Polar Caps of Mars. LPI Technical Report Number 87-01, Lunar and Planetary Institute, Houston, TX. adasbs.harvard.edu/full/1986LPICo.599...43I.

Iwasaki, K., Y. Saito, and T. Akabane. 1986b. Martian south polar cap 1973. Publ. Astron. Soc. Japan, 38, 267–275. adsabs.harvard.edu/abs/1986PASJ...38..267I.

Iwasaki, K., Y. Saito, Y. Nakai, T. Akabane, E. Panjaitan, I. Radiman and S.D. Wiramihardja. 1989. Behavior of the martian south polar cap 1986. Publ. Astron. Soc. Japan, 41, 1,083-1,094. adsabs.harvard.edu/full/1989PASJ...41.1083I.

Iwasaki, K., Y. Saito, Y. Nakai, T. Akabane, E. Panjaitan, I. Radiman and S.D. Wiramihardja. 1990. Martian south polar cap 1988. J. Geophys. Res., 95, 14,751–14,754. https://doi.org/10.1029/JB095iB09p14751.

James, P.B., B.A. Cantor, and S. Davis. 2001. Mars orbiter camera observations of the Martian south polar cap in 1999-2000. J. Geophys. Res., 106 (No. E10) 23,635–23,652. https://doi.org/10.1029/2000JE001313.

James, P.B. and K. Lumme, 1982. Martian south polar cap boundary: 1971 and 1973 Data. Icarus, 50, 368–380.https://www.sciencedirect.com/science/article/abs/pii/0019103582901300.

James, P.B., K.M. Malolepszy, and L.J. Martin. 1987. Interannual variability of Mars' south polar cap. Icarus, 71, 298–305. https://doi.org/10.1016/0019-1035(87)90154-0.

James, P.B., L.J. Martin, J.R. Henson, and P.V. Birch. 1990. Seasonal recession of Mars' south polar cap in 1986. J. Geophys. Res., 95, 1,337–1341. https://doi.org/10.1029/JB095iB02p01337.

Kieffer, H.H. 1979. Mars south polar spring and summer temperatures: a residual CO_2 frost. J. Geophys. Res., 84, 8263–8288. https://doi.org/10.1029/JB084iB14p08263.

Kieffer, H.H., T.N. Titus, K.F. Mullins, and P.R. Christensen. 2000. Mars south polar spring and summer behavior observed by TES: seasonal cap evolution controlled by frost grain size. J. Geophys. Res., 105(E4) 9,653–9,699. https://doi.org/10.1029/1999JE001136.

Kuiper, G.P. 1957. Visual observations of Mars, 1956. The Astrophysical Journal, 125, 307–317. adsabs.harvard.edu/full/1957ApJ...125..307K.

Larson, R. and B. Farber. 2006. Elementary Statistics. Pearson Education, Inc., Upper Saddle River, New Jersey. https://www.slader.com/textbook/9780131924956-elementary-statistics-3rd-edition/.

Lowell, P. 2002. Mars. reprinted from 1895 edition, Broham Press, Waterbury CT, plate II.

Malin, M.C., B.A. Cantor, and A.W. Britton. 2018a. MRO MARCI Weather Report for the week of 23–29 July 2018 Malin Space Science Systems Captioned Image Release MSSS-541 http://www.msss.com/msss_images/2018/08/01/.

Malin, M.C., B.A. Cantor, and A.W. Britton. 2018b. MRO MARCI Weather Report for the week of 30 July 2018–5 August 2018 Malin Space Science Systems Captioned Image Release MSSS-542 http://www.msss.com/msss_images/2018/08/08/.
McKim, R. 1984. The Opposition of Mars, 1980. J. Brit. Astron. Assoc., 94, 197–210. adsabs.harvard.edu/full/1984JBAA...94..197M.
McKim, R. 1985. The opposition of Mars, 1982. J. Brit. Astron. Assoc., 96, 36–52. adsabs.harvard.edu/full/1985JBAA...96...36M.
McKim, R. 1987. The opposition of Mars, 1984. J. Brit. Astron. Assoc., 97, 139–154. adsabs.harvard.edu/full/1987JBAA...97..139M.
McKim, R. 1989. The opposition of Mars, 1986. J. Brit. Astron. Assoc., 99, 215–232. adsabs.harvard.edu/full/1989JBAA...99..215M.
McKim, R. 1991. The opposition of Mars, 1988. J. Brit. Astron. Assoc., 101, 264–283. adsabs.harvard.edu/abs/1991JBAA..101..265M.
McKim, R. 1992. The opposition of Mars, 1990. J. Brit. Astron. Assoc., 102, 248–264. adsabs.harvard.edu/full/1992JBAA..102..248M.
McKim, R. 1995. The opposition of Mars, 1993. J. Brit. Astron. Assoc., 105, 117–134. adsabs.harvard.edu/full/1995JBAA..105..117M.
McKim, R. J. 1999. Telescopic Martian Dust Storms: A Narrative and Catalogue. Memoirs of the British Astronomical Association, 44, 1–165. https://www.britastro.org/node/10910.
McKim, R. 2005. The opposition of Mars, 1995. J. Brit. Astron. Assoc., 115, 313–333. adsabs.harvard.edu/full/2005JBAA..115..313M.
McKim, R. 2006. The opposition of Mars, 1997. J. Brit. Astron. Assoc., 116, 169–186. adsabs.harvard.edu/full/2006JBAA..116..169M
McKim, R. 2007. The opposition of Mars, 1999. J. Brit. Astron. Assoc., 117, 314–330. adsabs.harvard.edu/abs/2007JBAA..117..314M.
McKim, R. 2009. The opposition of Mars, 2001: Part I. J. Brit. Astron. Assoc., 119, 123–143. adsabs.harvard.edu/abs/2009JBAA..119..123M.
McKim, R. 2010a. The great perihelic opposition of Mars, 2003: Part I. J. Brit. Astron. Assoc., 120, 280–295. adsabs.harvard.edu/full/2010JBAA..120..280M.
McKim, R. 2010b. The great perihelic opposition of Mars, 2003: Part II. J. Brit. Astron. Assoc., 120, 347–357. adsabs.harvard.edu/full/2010JBAA..120..347M.
McKim, R. 2011. The opposition of Mars, 2005: Part I. J. Brit. Astron. Assoc., 121, 143–154. adsabs.harvard.edu/full/2011JBAA..121..143M.
McKim, R. 2012. The opposition of Mars, 2007: Part I. J. Brit. Astron. Assoc., 122, 207–219. adsabs.harvard.edu/abs/2012JBAA..122..207M.
McKim, R. 2018. The opposition of Mars, 2010: Part I. J. Brit. Astron. Assoc., 128, 157–167. adsabs.harvard.edu/abs/2018JBAA..128..157M.
NASA Photojournal website at https://photojournal.jpl.nasa.gov/catalog/P1A02998.
Piqueux, S., S. Byrne, H.H. Kieffer, T.N. Titus, and C.J. Hansen. 2015. Enumeration of Mars years and seasons since the beginning of telescopic exploration. Icarus, 251, 332–338. https://doi.org/10.1016/j.icarus.2014.12.014.
Schmude, R.W., Jr. 1989. Observations of Mars in 1988. J. Roy. Astron. Soc. Can., 83, 405–427. adsabs.harvard.edu/full/1989JRASC..83..405S.
Schmude, R.W., Jr. 2002. Photometric and Polarimetric Observations of Mars in 2000-2002. J. Roy. Astron. Soc. Can., 96, 105–110. adsabs.harvard.edu/abs/2002JRASC..96..105S.

Schmude, R.W., Jr. et al. 2004. ALPO Observations of the 2003 Apparition of Mars. J. Assoc. Lunar & Planet. Obs., 46(4), pp. 28–45. adsabs.harvard.edu/full/2004JALPO..46d..28S.

Schmude, R.W., Jr. 2017. ALPO Observations of Mars During the 2005 Apparition. J. Assoc. Lunar & Planet. Obs., 59(1) 58–72. adsabs.harvard.edu/abs/2016JALPO..59a..58s.

Schmude, R.W., Jr. 2018a. The North Polar Region of Mars in 2016. J. Assoc. Lunar & Planet. Obs., 60(2) 49–56. adsabs.harvard.edu/abs/2018JALPO..60b..49S.

Schmude, R.W., Jr. 2018b. The North Polar Hood of Mars. Journal of the British Astronomical Association, 128, 351–56. adsabs.harvard.edu/abs/2018JBAA..128..351S.

Schmude, R.W., Jr. 2018c. The North Polar Region of Mars: A Review. Proceedings for the 37th Annual Symposium on Telescopic Science & ALPO Annual Meeting. 115–131.

Schmude, R.W., Jr. 2019. Mars: The South Polar Hood and Hellas. J. Assoc. Lunar & Planet. Obs,. 61(1) 52–62.

Slipher, E. C. 1962. The Photographic Story of Mars. Sky Publishing Corp., Cambridge, MA.

Smith, M.D. 2004. Interannual variability in TES atmospheric observations of Mars during 1999–2003. Icarus, 167, 148-16. https://doi.org/10.1016/j.icarus.2003.09.010

Strom, R.G., S.K. Croft and N.G. Barlow. 1992. "The Martian Impact Cratering Record" in Mars (H.H. Kiefer, B.M. Jakosky, C.W. Snyder and M.S. Matthews—editors) University of Arizona Press, Tucson, pp. 383–423.

Titus, T.N. and H.H. Kieffer. 2002. A Comparison of the Mars South Polar Recession Rates Between 1999 and 2001. Lunar and Planetary Science Conference, XXXIII. https://www.lpi.usra.edu/meetings/lpsc2002/pdf/2071.pdf.

Venable, R. 2018. Report on the Mars Apparition of 2007-2008. J. Assoc. Lunar & Planet. Obs., 60(1) 48–99. adsabs.harvard.edu/abs/2017JALPO..60a..48V.

Veverka, J. and J. Goguen. 1973. The Nonuniform Recession of the South Polar Cap of Mars. Journal of the Royal Astronomical Society of Canada, 67, 273–290. adsabs.harvard.edu/full/1973JRASC..67..273V.

Wang, H. and A.P. Ingersoll. 2002. Martian clouds observed by Mars Global Surveyor Mars Orbiter Camera. Journal of Geophysical Research, 107, No. E10, 5078, https://doi.org/10.1029/2001JE001815.